Modeling and identification of the Quanser Aero using a detailed description of friction and centripetal forces

Mathias Dyvik[1] Didrik Efjestad Fjereide[1] Damiano Rotondo*[1]

[1]Department of Electrical and Computer Engineering (IDE), University of Stavanger, Stavanger, Norway
Corresponding author: damiano.rotondo@uis.no

Abstract

This paper deals with the modeling and identification of the Quanser Aero. The Quanser Aero is an aerospace laboratory setup designed for teaching aerospace concepts. Two propellers generate thrust and allow the user to control its dynamic response. The ability to lock axes individually makes it capable of abstracting a variety of aerospace systems, such as half-quadrotor, 1-Degree of freedom (DOF), vertical take-off and landing (VTOL), and 2-DOF helicopter. This paper focuses on the latter of these modes. In this configuration, the Quanser Aero can produce different pitch and yaw angles based on the angular velocity of the propellers, which produces an interesting identification and control problem, due to the presence of nonlinearities and significant cross-couplings between different variables. In this paper, a nonlinear model derived from Newton's law and Euler's rotational dynamics is obtained, and the unknown model parameters are identified through an experimental approach, with the model validated through real-time testing. In particular, it is shown that by means of a more detailed description of the friction, which includes the Karnopp's model that keeps the sum of the magnitude of all forces equal to zero until the applied forces are strong enough to overcome the friction force, and of the centripetal forces acting on the Aero, significant improvements are obtained when compared to state-of-the-art models. These improvements may hold the potential to enhance the performance of advanced nonlinear model-based control algorithms for this device.
Keywords: Quanser Aero, nonlinear model, friction

1 Introduction

With the advance of technology, aerial vehicles are steadily becoming more and more ubiquitous. For example, their unmanned versions, commonly referred to as *drones*, are widely used in several applications where it is either dangerous or economically inefficient to employ human pilots, e.g., for monitoring (Ren et al., 2019) and transport (Thiels et al., 2015) tasks. In order to train engineers to analyse the dynamical behaviour of aerial vehicles and design efficient and effective feedback control systems for them, small-scale devices that are apt to use in laboratories for educational purposes have been developed. These devices solve some of the most common issues encountered when unmanned aerial vehicles are applied to education, such as their limited autonomy and logistical/safety problems, among others (Shadiev and Yi, 2022). One of such devices is the Quanser Aero, a reconfigurable dual-rotor aerospace setup designed for teaching control and introducing aerospace concepts at an undergraduate level, but at the same time complex enough to enable its use in research, see e.g. (Kim and Ahn, 2021; Fliess and Join, 2022).

Attaining a satisfactory performance when controlling a highly coupled and nonlinear system such as the Quanser Aero is a challenging problem. It is known that nonlinear control algorithms are able to achieve better performance than linear control schemes (Kumar and Dewan, 2022), although they require a precise and reliable model that describes the system under consideration over a broad range of operating conditions. For this reason, several students and researchers have engaged in obtaining a model of the Quanser Aero that goes beyond the simple linear model provided by the manufacturer. For instance, (Frasik and Gabrielsen, 2018) have provided a nonlinear model calibrated through the analysis of free-oscillation and step responses. (Schlanbusch, 2019) derived a nonlinear mathematical model based on an Euler-Lagrange approach, where the uncertain parameters were updated in real-time by an adaptive control law.(Abdelwahed et al., 2019) used a reduced complexity autoregressive with exogenous input (ARX)-Laguerre model to describe the Quanser Aero in a selected operating point. (Segerstrom et al., 2021) used particle swarm optimization and constrained nonlinear optimization to obtain key electrical, mechanical and aerodynamical parameters for this device. (Kumar and Dewan, 2022) further improved the model and used it to design linear quadratic regulator (LQR) and sliding mode controller (SMC) algorithms.

In this paper, we obtain a nonlinear model using a Newton-Euler approach, identify its unknown parameters through an experimental approach, and validate the model through real-time testing. The main feature of the proposed model is a more detailed description of the friction, which includes the Karnopp's model, and of the centripetal forces acting on the Aero. Using different per-

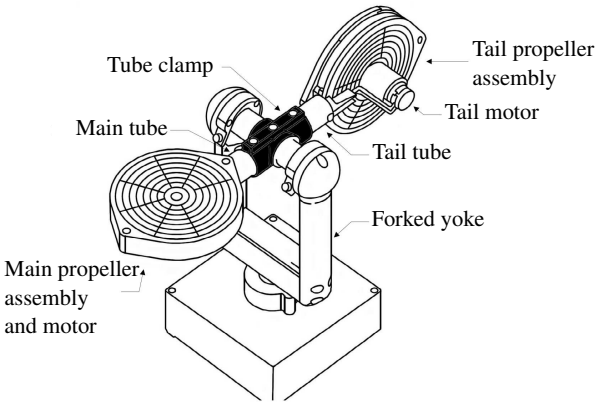

Figure 1. General component arrangement of the mechanical parts on the Quanser Aero. Adapted from (Qua, 2016)

formance indices under several operating conditions, we highlight significant improvements in the model's ability to capture the nonlinearities of the system in comparison with state-of-the-art models. Hence, the proposed model could potentially contribute significantly to the design of advanced nonlinear model-based control algorithms that require a stronger match between reality and model.

The remaining of this paper is structured as follows. Section 2 provides a description of the Quanser Aero. A detailed explanation of the mathematical model considered in this paper is given in Section 3. Section 4 presents the experimental comparison between the proposed model and other state-of-the-art models encountered in the literature. Finally, Section 5 summarizes the main conclusions of the work.

2 System description

The Aero is a dual-propeller laboratory setup designed for education and research in aerospace control, manufactured by Quanser Consulting Inc. It is equipped with two identical propellers, each of which is driven by a brushed direct-current (DC) motor. By applying motor voltages ranging within ± 18V, the user can manipulate the thrust produced by the propellers, thereby affecting the dynamics of the Aero. Moreover, the experiment is reconfigurable, meaning that the propeller assemblies can be tilted to desired angles. This, together with its ability to lock axes individually, allows the Aero to abstract various aerospace systems, such as half-quadrotor 1-DOF VTOL, and 2-DOF helicopter. This paper considers the latter case, where the propellers are perpendicular, as shown in Fig. 1.

The Quanser Aero can be considered as the composition of three structures: the base, the support yoke, and the helicopter body. The base is a stationary box at the bottom of the Aero and contains the electrical and electronic components necessary to control the system. The support yoke, shaped like a fork, stands vertically on the Aero base and serves to elevate the helicopter body, allowing it to rotate around its vertical axis. A rotational joint between the base and the yoke combined with a slip ring wiring system allows for an unlimited 360° yaw rotation. The helicopter body comprises two coupled metal tubes held together by a tube clamp, with a pair of propeller assemblies at both ends. It is horizontally attached to the forked yoke through a rotational joint, allowing the pitch angle of the helicopter body to rotate between -62° and $+54^\circ$.

Figure 2. 3D-printed low-efficiency (left) and high-efficiency (right) propellers (left)

The propeller pair in the Quanser Aero system is interchangeable. As of now, Quanser offers two types of propellers: high-efficiency and low-efficiency (see Fig. 2). This study considers the latter type. Although the high-efficiency propellers are more representative of small-scale aerial vehicles, a dynamic coupling between axes, which is seen in real aerial vehicles, is only present when the low-efficiency propellers are used. Thus, from a control engineering perspective, the use of low-efficiency propellers poses a more interesting and challenging problem.

The Aero setup is equipped with four optical rotary encoders that precisely measure the angular position of each DC motor, as well as the pitch and yaw angles of the helicopter body. An inertial measurement unit (IMU), which combines an accelerometer and a gyroscope, is also integrated into the Aero.

3 Mathematical Model

The mathematical model presented in this section describes the 2-DOF helicopter configuration of the Quanser Aero. It was derived by considering it as a rigid body and applying Newton's laws and Euler's rotational dynamics. The model is based on several electrical and mechanical parameters outlined in Table 1, most of which are provided by the manufacturer. Unknown parameters related to dynamical properties such as damping, friction, and propeller thrust have been experimentally identified and are listed in Table 2.

3.1 Propeller dynamics

The main and tail propeller dynamics are modeled as two nonlinear differential equations containing identical parameters:

$$\frac{\mathrm{d}\omega_p}{\mathrm{d}t} = \frac{K_\tau}{R_a J_{eq}} v_p - \frac{K_\tau K_E}{R_a J_{eq}} \omega_p - \frac{1}{J_{eq}} f_d(\omega_p) \tag{1}$$

Table 1. Known/ estimated physical parameters

Symbol	description	Value
Dc motor		
K_τ	Torque constant	$0.042\ Nm/a$
K_E	Motor back-emf constant	$0.042\ V/rad \cdot s$
R_a	Terminal resistance	$8.4\ \Omega$
J_{rotor}	Rotor inertia	$4.0 \times 10^{-6}\ kgm^2$
m_e	Mass of DC motor	$0.200\ kg$
Propeller		
J_{prop}	Low-efficiency propeller inertia	$3.2 \times 10^{-5}\ kgm^2$
J_{hub}	Propeller hub inertia	$3.04 \times 10^{-9}\ kgm^2$
m_{pa}	Mass of propeller assembly	$0.146\ kg$
Helicopter body		
m_b	Total mass of helicopter body	$1.15\ kg$
m_{mt}	Mass of main propeller tube	$0.089\ kg$
m_{tt}	Mass of tail propeller tube	$0.089\ kg$
m_{tc}	Mass of tube clamp	$0.280\ kg$
l_t	Length of tubes and tube clamp when assembled	$0.165\ m$
d_t	Thrust displacement	$0.158\ m$
d_m	Aero body vertical COM displacement	$0.00325\ m$
d_c	Main/tail section horizontal COM displacement	$0.106\ m$
Forked yoke		
m_y	Mass of the forked yoke	$0.526\ kg$
r_y	Radius of the forked yoke	$0.02\ m$

$$\frac{\mathrm{d}\omega_y}{\mathrm{d}t} = \frac{K_\tau}{R_a J_{eq}} v_y - \frac{K_\tau K_E}{R_a J_{eq}} \omega_y - \frac{1}{J_{eq}} f_d(\omega_y) \tag{2}$$

where $v_{p/y}$ is the input voltage of the main/tail motor, $\omega_{p/y}$ is the angular velocity of the main/tail propeller, and J_{eq} is the total moment of inertia of the main/tail propeller subsystem.

The torques exerted by the DC motors on the propeller shafts can be modelled as the product of a torque constant, K_τ, and the applied armature currents, $i_{ap/y}$:

$$\tau_{mp/y} = K_\tau i_{ap/y} \tag{3}$$

The armature current can then be expressed in terms of the input voltages by applying Kirchhoff's voltage law:

$$i_{ap/y} = \frac{v_{p/y}}{R_a} - \frac{L_a}{R_a} \frac{di_{ap/y}}{dt} - \frac{e_b}{R_a} \tag{4}$$

where R_a is the motor armature resistance, L_a is the motor inductance, and $e_b = K_E \omega_{p/y}$ is the back-emf voltage which depends on the angular velocity of the propeller shafts. As suggested by the Quanser laboratory guide, (4) can be simplified by neglecting electrical dynamics, i.e., setting the motor inductance equal to zero (Qua, 2016). Furthermore, the Quanser lab guide proposes modeling the torque exerted by drag and air resistance as linear functions of propeller angular velocities:

$$\tau_d = k_d \omega_m \tag{5}$$

where k_d is an experimentally derived torque constant. However, online experiments conducted on the Aero's main propeller have shown that the following non-linear function provides a more accurate representation of the drag and air resistance:

$$\begin{aligned} \tau_d = f_d(\omega_{p/y}) = sign(\omega_{y/p}) k_{d1} \omega_{p/y}^2 \\ + k_{d2} \omega_{p/y} + sign(\omega_{y/p}) k_{d3} \end{aligned} \tag{6}$$

Table 2. Experimentally identified parameters

Parameter	Value	Parameter	Value
k_{Mpp_1}	1.69×10^{-6}	k_{Typ_1}	1.06×10^{-6}
k_{Mpp_2}	9.65×10^{-7}	k_{Typ_2}	1.17×10^{-5}
k_{Mpn_1}	-2.55×10^{-6}	k_{Tyn_1}	-1.41×10^{-6}
k_{Mpn_2}	-4.69×10^{-5}	k_{Tyn_2}	-4.16×10^{-5}
k_{Myp_1}	7.30×10^{-7}	k_{Tpp_1}	1.66×10^{-6}
k_{Myp_2}	-1.61×10^{-5}	k_{Tpp_2}	-2.83×10^{-5}
k_{Myn_1}	-6.43×10^{-7}	k_{Tpn_1}	-1.63×10^{-7}
k_{Myn_2}	3.28×10^{-5}	k_{Tpn_2}	8.37×10^{-6}
k_{d_1}	2.90×10^{-7}	k_{Dyp_1}	1.84×10^{-5}
k_{d_2}	4.20×10^{-6}	k_{Dyp_2}	3.64×10^{-4}
k_{d_3}	8.00×10^{-4}	k_{Dyn_1}	-5.05×10^{-5}
k_{Fyp}	4.98×10^{-3}	k_{Dyn_2}	9.86×10^{-4}
k_{Fyn}	-2.90×10^{-3}	k_{Dp_1}	7.10×10^{-3}
k_{Fp}	2.00×10^{-4}		

where k_{d1}, k_{d2}, and k_{d3} are torque constants identified by iterative online tuning.

The total moment of inertia, J_{eq}, has been modeled according to the Quanser laboratory documentation as:

$$J_{eq} = J_{prop} + J_{hub} + J_{rotor} \tag{7}$$

where J_{prop} denotes the moment of inertia of the propeller, J_{hub} represents the moment of inertia acting on the clamp used to mount the propeller to the motor, and J_{rotor} is the moment of inertia of the DC motor shaft. The specific values for J_{hub} and J_{rotor} can be obtained from the Quanser laboratory documentation. However, the moment of inertia for the propeller, J_{prop}, is only provided for the high-efficiency propeller. The moment of inertia for the low-efficiency propeller has therefore been estimated using the computer-aided design (CAD) software *Autodesk Inventor*.

The resulting propeller velocity model (1)-(2) is obtained by considering equations (3), (6) and (7), and applying Newton's second law for rotation: $J\ddot{\theta} = \sum_i \tau_i$.

3.2 Pitch motion

The model describing the Aero's pitch movement is expressed as:

$$\begin{aligned} \frac{\mathrm{d}\Omega_p}{\mathrm{d}t} = & \frac{f_{Mp}(\omega_p) d_t + f_{Tp}(\omega_y) d_t - m_b g d_m \sin(\theta_p)}{J_p} \\ & - \frac{(m_A + m_B) \Omega_y^2 d_c^2 \cos(\theta_p) \sin(\theta_p)}{J_p} \\ & - \frac{f_{Dp}(\Omega_p) - f_{Fp}(\Omega_p)}{J_p} \end{aligned} \tag{8}$$

$$\frac{\mathrm{d}\theta_p}{\mathrm{d}t} = \Omega_p \tag{9}$$

where Ω_p is the angular velocity in the pitch direction, θ_p is the pitch angle and J_p is the moment of inertia about the pitch axis.

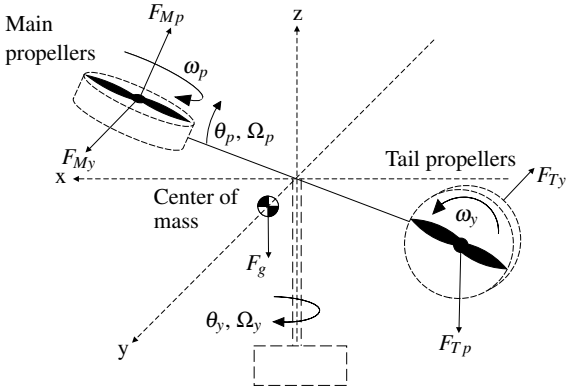

Figure 3. Free body diagram of the Quanser Aero 2-DOF helicopter configuration.

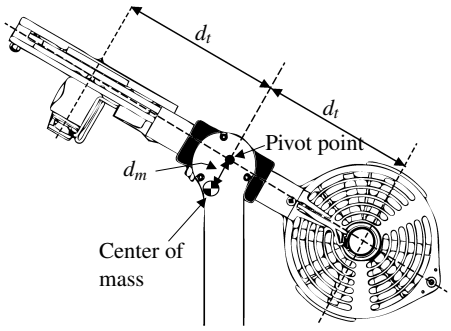

Figure 4. Center of mass and thrust displacement. Adapted from (Qua, 2016)

Fig. 3 shows a free-body diagram illustrating the forces acting on the Aero. In the 2-DOF helicopter configuration, the main propeller is fixed horizontally and produces a vertical thrust force F_{Mp} that enables the Aero to pitch. However, the main propeller also produces a perpendicular force F_{My}, which produces a cross-torque and thus a negative yaw rotation. The tail propeller is fixed vertically and is mainly used to counteract the cross-torque caused by the main propeller. The predominant thrust force from the tail propeller, which causes positive yaw rotation, is denoted by F_{Ty}. Similar to the main propeller, the tail propeller produces an additional perpendicular force F_{Tp}, which causes a positive rotation about the pitch axis. The gravitational pull F_g acts on the centre of mass (COM) of the helicopter body, which is slightly below its pivot point, so that the helicopter body acts like a pendulum. This implies that the pitch angle of the Aero returns to a horizontal equilibrium position if no force is applied. Fig. 4 illustrates the COM displacement d_m, which varies with how the propeller assemblies are angled. Unfortunately the documentation provided by Quanser Inc. gives the COM displacement only for the 1-DOF VTOL configuration. (Frasik and Gabrielsen, 2018) estimated this value to be $2.7mm$ for the 2-DOF helicopter configuration, whereas (Schlanbusch, 2019) suggest a higher value $3.8mm$. Our testing suggests that using the mean of the aforementioned values results in a satisfactory representation of the real system.

The torque induced by the gravitational force, which affects the pitch movement, is derived by multiplying the gravitational force F_g with the moment arm $d_m \sin(\theta_p)$:

$$\tau_g = F_g d_m \sin(\theta_p) = m_b g d_m \sin(\theta_p) \tag{10}$$

where m_b is the mass of the helicopter body.

The predominant thrust force of the main propeller F_{Mp} and the cross-thrust of the tail propeller F_{Tp} have been estimated using the experimental procedure proposed in (Schlanbusch, 2019). This method involves accelerating the propeller of interest to various rotational velocities while the other propeller remains disengaged, with the yaw axis locked, thus reducing the Aero setup to a 1-DOF system. The resulting steady-state pitch angles are then measured to obtain estimates of the thrust forces. With only the main/tail propeller engaged, the pitch angle at steady state, and the yaw axis locked, the equation of motion about the pitch axis with respect to $F_{Mp/Tp}$ becomes:

$$F_{Mp/Tp} = \frac{m_b d_m \sin(\theta_p)}{d_t} \tag{11}$$

where d_t is the thrust displacement of the Aero illustrated in Fig. 4. Then with the use of a least square approach, it was found that the following nonlinear piecewise functions provided a more accurate representation of the thrust forces:

$$F_{Mp} = f_{Mp}(\omega_p) = \begin{cases} k_{Mpp_1}\omega_p^2 + k_{Mpp_2}\omega_p & \text{if } \omega_p \geq 0 \\ k_{Mpn_1}\omega_p^2 + k_{Mpn_2}\omega_p & \text{if } \omega_p < 0 \end{cases} \tag{12}$$

$$F_{Tp} = f_{Tp}(\omega_y) = \begin{cases} k_{Tpp_1}\omega_y^2 + k_{Tpp_2}\omega_y & \text{if } \omega_y \geq 0 \\ k_{Tpn_1}\omega_y^2 + k_{Tpn_2}\omega_y & \text{if } \omega_y < 0 \end{cases} \tag{13}$$

The Coulomb friction opposing the pitch movement is modelled using a static friction coefficient:

$$F_{Fp} = f_{Fp}(\Omega_p) = sign(\Omega_p) k_{Fp} \tag{14}$$

while a linear function identified by Quanser (Qua, 2016) has been implemented for the pitch damping:

$$f_{Dp}(\Omega_p) = k_{Dp_1}\Omega_p \tag{15}$$

where k_{Dp_1} is a damping coefficient.

As the Aero undergoes a yaw rotation, the helicopter body's ends trace a spherical path. This implies that the main and tail sections will experience a centripetal force directed toward the centre of curvature, forcing the pitch position toward its horizontal equilibrium. The centripetal force acting on the main/tail part of the helicopter body can be expressed as:

$$F_{cm/t} = m_{A/B}\Omega_y^2 d_c \cos(\theta_p) \tag{16}$$

where $m_A = \frac{m_{tc}}{2} + m_{mt} + m_e + m_{pa}$ and $m_B = \frac{m_{tc}}{2} + m_{tt} + m_e + m_{pa}$, d_c is the length from the pivot point to the total

COM of the main/tail tube, main/tail propeller assembly, and half of the tube clamp. This distance has been calculated based on the dimensions of the tube clamp, which measures approximately 90mm, the length of each tube, which is around 130mm, and the distance from the pivot point to the centre of each propeller assembly, which is 158mm. The net torque produced by the vertical component of the centripetal forces acting on the tail and main sections of the Aero has been derived following the approach described in (Christensen et al., 2006), which involves a comprehensive analysis of a similar small-scale aerospace device. The resulting net centripetal torque is expressed as:

$$\tau_{Cp} = -(m_A + m_B)\Omega_y^2 d_c^2 \cos(\theta_p)\sin(\theta_p) \tag{17}$$

The resulting pitch motion model (8) is obtained by considering equations (10), (12)-(15), (17) and (31), and applying Newton's second law for rotation. Note that the torques produced by the thrust forces in (12) and (13) are computed by multiplying the forces by the moment arm d_t.

3.3 Yaw motion

The model describing the Aero's yaw movement is expressed as:

$$\frac{\mathrm{d}\Omega_y}{\mathrm{d}t} = \frac{f_{Ty}(\omega_y)\cos(\theta_p)d_t - f_{My}(\omega_p)\cos(\theta_p)d_t}{J_y(\theta_p)} - \frac{f_{Dy}(\Omega_y) - f_{Fy}(\Omega_y, F_{My}, F_{Ty})}{J_y(\theta_p)} \tag{18}$$

$$\frac{\mathrm{d}\theta_y}{\mathrm{d}t} = \Omega_y \tag{19}$$

where Ω_y is the angular velocity in the yaw direction, θ_y is the yaw angle, and $J_y(\theta_p)$ is the moment of inertia about the yaw axis.

The predominant thrust force of the tail propeller F_{Ty} and the cross-thrust of the main propeller F_{Mp} follow the same model as (12) and (13):

$$F_{My} = f_{My}(\omega_p) = \begin{cases} k_{Myp1}\omega_p^2 + k_{Myp2}\omega_p & \text{if } \omega_p \geq 0 \\ k_{Myn1}\omega_p^2 + k_{Myn2}\omega_p & \text{if } \omega_p < 0 \end{cases} \tag{20}$$

$$F_{Ty} = f_{Ty}(\omega_y) = \begin{cases} k_{Typ1}\omega_y^2 + k_{Typ2}\omega_y & \text{if } \omega_y \geq 0 \\ k_{Tyn1}\omega_y^2 + k_{Tyn2}\omega_y & \text{if } \omega_y < 0 \end{cases} \tag{21}$$

As the propellers are identical, it can be assumed that the parameters identified for f_{Mp} and f_{Tp} are representative for f_{Ty} and f_{My}, respectively. However, real-time testing indicated that this assumption resulted in more thrust than needed for the yaw movement due to unmodeled dynamics. Slightly down-tuned versions of the vertical thrust force functions are therefore implemented for the horizontal thrust force functions.

The viscous damping acting about the yaw axis, $f_{Dy}(\Omega_y)$ has been estimated by examining free-oscillation responses, as proposed in (Qua, 2016). To obtain the free-oscillation responses, the Aero was decelerated from various yaw velocities with both propellers disengaged and the pitch axis locked in its horizontal equilibrium position. By approximating the yaw deceleration as $\frac{\Delta\Omega_y}{\Delta t}$, (18) reduces to:

$$\frac{\Delta\Omega_y}{\Delta t} = -\frac{f_{Dy}(\Omega_y) + F_{Fy}}{J_y(0)} \tag{22}$$

where F_{Fy} is the static friction force opposing the yaw rotation. Then, by applying a least square regression to the measured data, a relationship between the angular yaw velocity and the sum of yaw damping and friction was obtained. The damping and friction have been distinguished by modeling the viscous damping using the regression coefficients and the static friction as the regression constant, as suggested in (Frasik and Gabrielsen, 2018), resulting in the following yaw damping function:

$$f_{Dy}(\Omega_y) = \begin{cases} k_{Dyp_1}\Omega_y^2 + k_{Dyp_2}\Omega_y & \text{if } \Omega_y \geq 0 \\ k_{Dyn_1}\Omega_y^2 + k_{Dyn_2}\Omega_y & \text{if } \Omega_y < 0 \end{cases} \tag{23}$$

and static friction force :

$$F_{Fy} = \begin{cases} k_{Fyp} & \text{if } \Omega_y > 0 \\ k_{Fyn} & \text{if } \Omega_y < 0 \end{cases} \tag{24}$$

However, during real-time testing of the Aero system, it was observed that the specific values obtained for the parameters $k_{Fyp/n}$ from the aforementioned experiment were too high. As a result, the parameter k_{Fyp} has been reduced by 20% and k_{Fyn} by 35%. Furthermore, to ensure that the net force acting on the yaw axis remains zero until the applied forces exceed the friction force, a friction modeling technique known as Karnopp's model has been implemented. In this way, the basic friction model in (24) can be extended to be valid at zero yaw velocity (Egeland and Gravdahl, 2002):

$$f_{Fy}(\Omega_y, F_{My}, F_{Ty}) = \begin{cases} sat(F_{Ty} - F_{My}, F_{Fy}) & \text{when } \Omega_y = 0 \\ F_{Fy} & \text{else} \end{cases} \tag{25}$$

where $sat()$ refers to the saturation function.

The resulting yaw motion model (18), is obtained by considering equations (20)-(21), (23), (25)-(26), and applying Newton's second law for rotation. Here, the torque produced by the thrust forces in (12) and (13) are computed by multiplying the thrust force by the moment arm $\cos(\theta_p)d_t$.

3.4 Moment of Inertia about the pitch and yaw axes

The total moments of inertia about the pitch/yaw axes J_p and J_y have been obtained as suggested in the laboratory documentation provided by Quanser Inc. However, by applying a more detailed description of the mass of the different mechanical components of the Aero, slightly lower numerical values for both the pitch and yaw inertia were obtained, which produced better results when the model

was tested against the actual plant. The components used in these estimates are shown in Fig. 1. Furthermore, Quanser's documentation ignores the fact that yaw inertia decreases with increasing pitch angle due to the mass being more concentrated along the vertical axis. Therefore, the yaw inertia is modelled as the nonlinear function of the pitch angle $J_y(\theta_p) = k_{Jy} f_{ky}(\theta_p)$, where k_{Jy} is the moment of inertia corresponding to a pitch angle of zero. In (Frasik and Gabrielsen, 2018) it was discovered that the nonlinear dynamics of the moment of inertia about the yaw axis are well described by a cosine function, resulting in the expression:

$$J_y(\theta_p) = k_{Jy}\cos(\theta_p) \tag{26}$$

The moments of inertia of the tubes and tube clamp connecting the main and tail propeller assemblies can be modelled as a solid cylinder perpendicular to the axis of rotation, rotating about its centre, resulting in:

$$J_{cylinder} = \frac{1}{12}(m_{mt} + m_{tt} + m_{tc})l_t^2 \tag{27}$$

By considering the two propeller assemblies as single-point masses rotating at a distance d_t from the pivot point of the helicopter body, their moment of inertia can be estimated as:

$$J_{pa} = (m_{pa} + m_e)d_t^2 \tag{28}$$

The forked yoke used to raise the helicopter body from the Aero base can be modelled as a solid cylinder rotating about its centre which leads to the expression:

$$J_{yoke} = \frac{1}{2}m_y r_y^2 \tag{29}$$

The total moment of inertia about the yaw axis with a fixed pitch angle of zero degrees is then obtained by summing (27), (28) and (29):

$$J_y(\theta_p = 0) = k_{Jy} = J_{cylinder} + 2J_{pa} + J_{yoke} \tag{30}$$

The total moment of inertia about the pitch axis is found as the sum of (27) and (28):

$$J_p = J_{cylinder} + 2J_{pa} \tag{31}$$

4 Experimental results

The purpose of the experiments described in this section was to test the model's ability to accurately predict the pitch angle, pitch velocity, yaw angle, and yaw velocity of the system when subjected to different input signals. To evaluate the performance of the model under various operating conditions, the input signal to the system was either varied in amplitude by changing the voltage level, or shifted in time by altering the step time. A total of twelve different input sequences were investigated, as shown in Fig. 5. For each sequence, ten different experiments have been performed and the average integral absolute errors (IAE) and integral square errors (ISE) of the model versus the plant were computed for the pitch and yaw velocities.

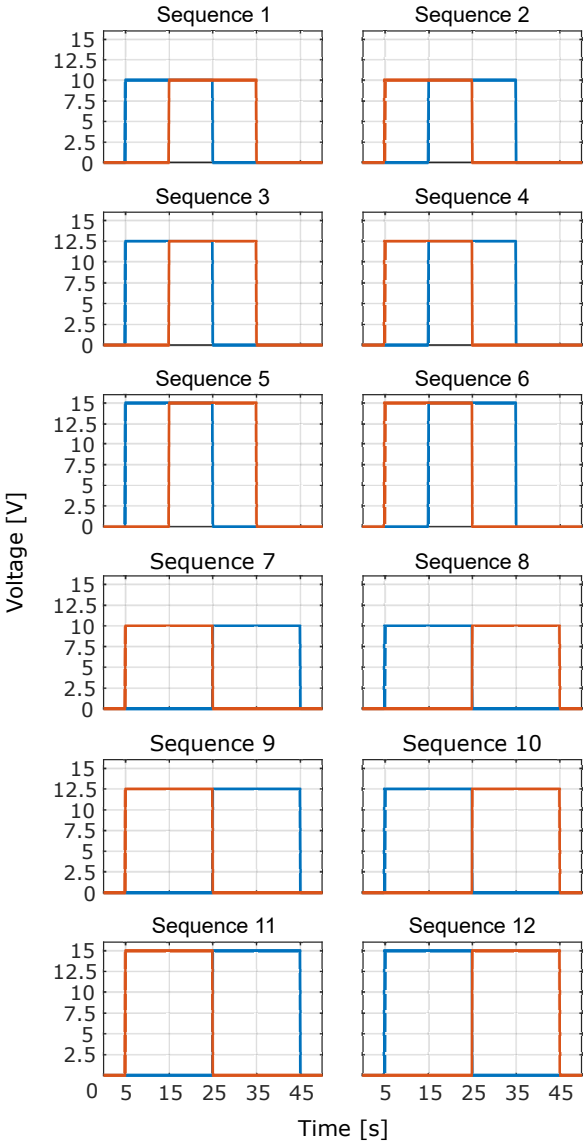

Figure 5. Input signal sequences

The performance of the model proposed in this paper compared to other state-of-the-art models in accurately predicting pitch angle, pitch velocity, yaw position, and yaw velocity, have been evaluated. Table 3 summarises the average IAE and ISE obtained for all input sequences. Fig. 6 shows the results in one particular run of input sequence number 3.

The results in the table show that, in the majority of experiments, the proposed model was either the best (dark green) or the second best (light green) model. Further examination of Table 3 reveals that the most significant improvement relates to the ability of the proposed model to predict yaw velocity. This is also evident in the plots presented in Figs. 6c and 6f. We can mention that the case of input sequence number 6, for which the yaw model underperformed, is the only observed exception. The improved performance of the proposed model with respect to predicting pitch motion, evident in Table 3, is primarily due to a more accurate representation of the frequency of oscillation and damping.

Table 3. Performance comparison of analysed models. The values are the average criteria after ten runs. Dark green color marks the highest performing model, and light green color marks the second highest performing model.

Sequence	Criteria		Frasik & Gabrielsen	Kumar & Dewan	Schlanbusch	Quanser	Dyvik & al.
1	dPitch	IAE	2.49	6.68	3.43	5.26	2.17
		ISE	0.28	1.47	0.39	1.07	0.21
	dYaw	IAE	14.95	20.84	24.63	20.84	3.94
		ISE	11.70	18.29	23.26	18.30	1.01
2	dPitch	IAE	3.07	6.64	3.44	4.94	2.19
		ISE	0.46	1.51	0.47	0.94	0.27
	dYaw	IAE	16.03	22.02	25.21	22.03	3.24
		ISE	12.78	20.30	24.49	20.31	0.66
3	dPitch	IAE	5.15	8.45	5.77	12.21	4.16
		ISE	0.94	2.38	1.55	5.88	0.77
	dYaw	IAE	30.62	20.61	21.80	20.62	6.73
		ISE	40.64	17.83	20.72	17.84	3.70
4	dPitch	IAE	6.62	8.52	4.28	8.65	3.83
		ISE	1.55	2.67	0.70	3.03	0.55
	dYaw	IAE	32.23	21.03	21.84	21.04	11.26
		ISE	42.76	19.33	22.28	19.34	6.53
5	dPitch	IAE	10.29	10.41	16.57	22.57	7.85
		ISE	4.04	3.98	12.19	25.36	2.70
	dYaw	IAE	48.51	26.81	21.75	26.82	8.13
		ISE	88.65	27.93	18.24	27.94	2.92
6	dPitch	IAE	10.86	9.22	16.23	19.24	6.23
		ISE	4.54	3.13	12.55	18.66	1.41
	dYaw	IAE	54.31	25.94	21.77	25.95	27.50
		ISE	101.07	27.04	18.39	27.06	41.20
7	dPitch	IAE	2.47	3.68	2.29	4.14	1.59
		ISE	0.31	0.58	0.25	0.75	0.16
	dYaw	IAE	46.80	39.83	42.84	39.84	11.15
		ISE	63.54	41.12	48.85	41.13	4.79
8	dPitch	IAE	2.22	3.44	1.97	3.45	1.76
		ISE	0.31	0.63	0.18	0.59	0.19
	dYaw	IAE	43.52	34.18	37.79	34.19	9.39
		ISE	56.18	33.95	43.36	33.96	2.59
9	dPitch	IAE	5.81	5.42	3.79	5.48	3.70
		ISE	1.43	1.28	0.68	1.51	0.77
	dYaw	IAE	71.47	39.67	40.42	39.68	23.00
		ISE	152.45	47.89	52.39	47.91	19.73
10	dPitch	IAE	4.77	4.61	3.75	5.64	3.01
		ISE	0.89	1.13	0.88	2.01	0.51
	dYaw	IAE	70.71	36.88	35.08	36.89	20.58
		ISE	170.88	37.67	40.93	37.68	13.51
11	dPitch	IAE	10.58	6.48	5.56	6.27	5.62
		ISE	3.86	2.01	1.44	2.48	1.41
	dYaw	IAE	99.85	51.09	47.52	51.10	42.14
		ISE	302.88	84.77	64.22	84.81	80.97
12	dPitch	IAE	10.31	6.09	4.65	5.06	3.05
		ISE	3.55	2.21	1.21	2.01	0.52
	dYaw	IAE	97.20	46.88	37.58	46.90	28.14
		ISE	320.08	71.30	41.64	71.33	25.43

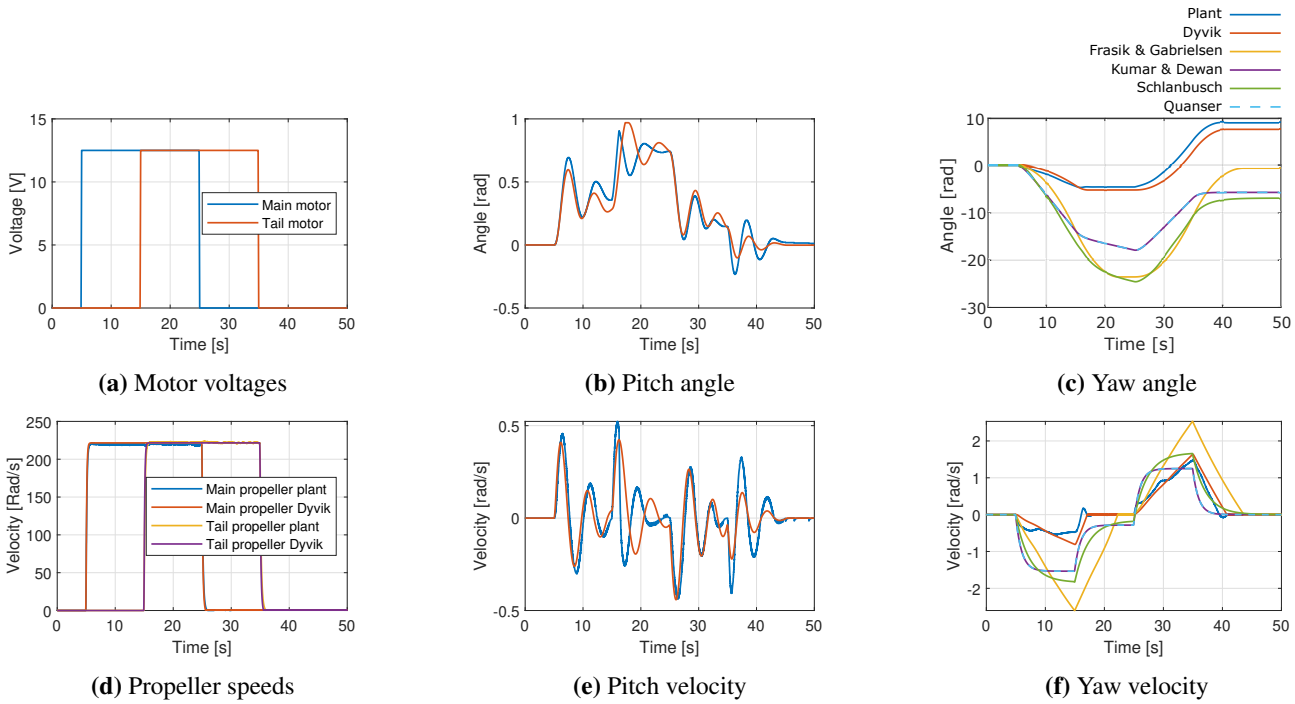

(a) Motor voltages **(b)** Pitch angle **(c)** Yaw angle

(d) Propeller speeds **(e)** Pitch velocity **(f)** Yaw velocity

Figure 6. Experiment 3 results. Note that Figs. 6b and 6e contain only the proposed model due to the possible interpretational challenges that arise from the fact that all the considered models oscillate with slightly different frequencies and amplitudes.

5 Conclusions

This paper has proposed an improved model for describing the dynamical behavior of a Quanser Aero 2-DOF helicopter equipped with inefficient propellers. The model includes a more detailed description of friction and centripetal forces acting on the Aero. An extensive experimental validation using different input sequences has shown that the improved model provides better results, in the sense of lower values for IAE and ISE criteria, than other models proposed in the literature.

References

I. B. Abdelwahed, A. Mbarek, and K. Bouzrara. Model predictive control of 2-DOF helicopter based on MIMO ARX-Laguerre model. In *6th International Conference on Electrical and Electronics Engineering (ICEEE)*, pages 317–322, 2019.

R Christensen, N Fogh, RH Hansen, MS Jensen, S Larsen, and A Paramanathan. Modelling and control of a twin-rotor mimo system. *Department of Control Engineering Institute of Electronic Systems of Aalborg University*, 2006.

O. Egeland and J. T. Gravdahl. *Modeling and simulation for automatic control*. Marine Cybernetics Trondheim, 2002.

M. Fliess and C. Join. An alternative to proportional-integral and proportional-integral-derivative regulators: intelligent proportional-derivative regulators. *International Journal of Robust and Nonlinear Control*, 32(18):9512–9524, 2022.

J. M. Frasik and S. I. Lund Gabrielsen. Practical application of advanced control: An evaluation of control methods on a quanser aero. Master's thesis, Universitetet i Agder, 2018.

S.-K. Kim and C. K. Ahn. Performance-boosting attitude control for 2-DOF helicopter applications via surface stabilization approach. *IEEE Transactions on Industrial Electronics*, 69(7):7234–7243, 2021.

S. Kumar and L. Dewan. A comparative analysis of LQR and SMC for Quanser AERO. In *Control and Measurement Applications for Smart Grid: Select Proceedings of SGESC*, pages 453–463. 2022.

Quanser AERO - Laboratory Documentation. Quanser Inc, 2016.

H. Ren, Y. Zhao, W. Xiao, and Z. Hu. A review of UAV monitoring in mining areas: Current status and future perspectives. *International Journal of Coal Science & Technology*, 6:320–333, 2019.

S. M. Schlanbusch. Adaptive backstepping control of quanser 2DOF helicopter: Theory and experiments. Master's thesis, Universitetet i Agder, 2019.

E. Segerstrom, M. Podlaski, A. Khare, and L. Vanfretti. Parameter optimization and model validation of Quanser Aero using Modelica and RaPId. In *AIAA/IEEE Electric Aircraft Technologies Symposium (EATS)*, pages 1–9, 2021.

R. Shadiev and S. Yi. A systematic review of UAV applications to education. *Interactive Learning Environments*, pages 1–30, 2022.

C. A. Thiels, J. M. Aho, S. P. Zietlow, and D. H. Jenkins. Use of unmanned aerial vehicles for medical product transport. *Air medical journal*, 34(2):104–108, 2015.